lengths longer than 1.5 μm show a reduction, as expected for long channels. Figure 6 shows normalized transfer characteristics for low threshold FET's of different channel lengths, with the maximum transconductances obtained at the inflection point. The highest value obtained was 465 mS/mm, with an associated voltage gain of 39.5 for a 0.75 μm opening in the chrome mask and 0.5 μm estimated channel length. The high voltage gain demonstrates that no extended high field domain is needed at the drain end of the channel to improve current confinement, as this is already provided by the (Al,Ga)As/GaAs junction.

The second parasitic effect investigated is the I-V collapse. HEMT devices using the AlGaAs/GaAs material system have been widely plagued with the phenomenon of the collapse of the I-V characteristics at low temperatures in the dark, applying high drain bias (2). This has been associated with electron trapping at deep donor centers ("DX"-centers) in (Al,Ga)As. A high field is needed, so that the electrons can surmount the repulsive barrier surrounding the center before being trapped, the high field being provided in a high field domain region in the *N*-doped (Al,Ga)As adjacent to the gate metal at the drain side outside the intrinsic device region. The I-V collapse should, thus, not be related to the intrinsic device structure, and be absent in HEMT structures with a narrow recess structure as described above. Figure 7 shows curve tracer output characteristics of a 1 μm HEMT at room temperature (7a), 77 K in light (7b), and at 77 K in dark (cooled down in dark) (7c). No instability leading to the I-V collapse is observed, although the threshold voltage shift of approximately 0.40V indicates a large percentage of "DX"-centers in the (Al,Ga)As.

Conclusion

Specific characteristics of the chemical etching of heterostructure (Al,Ga)As/GaAs material have been described. It is shown that a number of recess profiles can be obtained and narrow recess HEMT structures can be produced with the channel length smaller than the gate length. The major parasitic material effects, masking short channel device behavior, could be eliminated in devices of 0.3 μm gate length. These are channel current limiting effects, due to surface depletion, and the I-V collapse phenomenon, due to a high field domain in the (Al,Ga)As layer. It is expected that by tighter control of processing parameters and the use of high resolution lithography, devices with essentially negligible parasitics, in the 100 nm range and below, can be fabricated. Thus, it seems that wet chemical etching, especially when using low etch rates, can be very useful in achieving high vertical and lateral resolution in the processing of submicron 3-dimensional devices. Moreover, wet etching does not suffer from the electrical damage introduced by dry etching.

Acknowledgment

Sincere thanks to K. Hofmann for many stimulating discussions on short channel and parasitic device aspects, and to R. Bernadi, W. Wiegmann, L. Harner, and T. Jones for materials preparation and assistance in device processing. We also thank K. Zaininger for his steady support of this project.

Manuscript submitted on Feb. 24, 1987. This was Paper 769 SOA presented at the San Diego, CA, Meeting of the Society, Oct. 19-24, 1986.

SIEMENS Research and Technology Laboratories assisted in meeting the publication costs of this article.

REFERENCES

1. K. R. Hofmann, R. J. Cheponis, C. L. Shieh, K. Alavi, and E. Kohn, Presented at the SDHT-Conference, Hawaii, Dec. 1-6, 1986.
2. A. Kastalsky and R. A. Kiehl, *IEEE Trans. Electron Devices*, **ED-33**, 414 (1986).
3. U. K. Mishra, S. C. Palmateer, P. C. Chao, P. M. Smith, and J. C. M. Hwang, *IEEE Electron Devices Lett.*, **EDL-6**, 142 (1986).
4. E. Kohn, *This Journal*, **127**, 505 (1980).
5. H. M. Macksey, *IEEE Electron Device Lett.*, **EDL-7**, 69 (1986).
6. E. Kohn, *Electron. Lett.*, **11**, 160 (1975).
7. M. Schneider, C. Colvard, K. Alavi, and E. Kohn, *SPIE Proc.*, 797 (1987), Paper 797-12.

Laser Chemical Vapor Deposition of Gold

The Effect of Organometallic Structure

Thomas H. Baum

IBM Almaden Research Center, San Jose, California 95120-6099

ABSTRACT

The laser-induced pyrolytic deposition (LCVD) of gold from dimethylgold acetylacetonate and two fluorinated derivates has been examined. The incorporation of fluorine substituents on the acetylacetonate ligand increases the vapor pressure of the organogold complex substantially. Rates of gold deposition are strongly dependent upon the vapor pressure and therefore, the gold complex utilized. Rates of deposition, deposit resistivities, and deposit purities are compared for each of the gold complexes.

The laser-induced deposition of gold has been reported from plating solutions (1), metallo-organic films (2), and from the LCVD of dimethylgold acetylacetonate (3). The latter approach is a completely dry, single-step process in which the rates of metal film formation can be influenced by increasing the partial pressure of the organometallic precursor or by the addition of a buffer gas. The localized deposition of metal, which can be achieved by LCVD, enables one to fabricate, repair, or modify circuits, and repair clear defects in lithographic masks.

Laser chemical vapor deposition (LCVD) of metals is a modification of conventional CVD, in which a focused laser is absorbed by the substrate and utilized as a localized heat source. An organometallic, adsorbed or colliding with the surface, undergoes a thermal decomposition to metal with the liberation of volatile reaction products. The surface temperature profile, induced by laser heating of the substrate, defines the reaction zone and controls the deposition of metal. The optical and thermophysical properties of the substrate and deposited material are thus important process parameters. Another critical component to LCVD is the organometallic complex used as the metal precursor. The decomposition temperature of the organometallic will determine the laser power necessary for the initiation of deposition and the vapor pressure will profoundly influence the deposition rates. An ideal precursor will decompose cleanly to metal, in a selective manner, be stable at room temperature and in air. The thermal chemistry is extremely important for other reasons as well; a low decomposition temperature facilitates the deposition of metal onto thermally sensitive substrates (*i.e.*, polymers) without damage.

The role of precursor properties will be illustrated in this paper by examining the pyrolytic, vapor-phase deposition of high purity gold metal from dimethylgold(III) acetylacetonate, $Me_2Au(acac)$, and two fluorinated derivatives. These three complexes possess similar decomposition temperatures, are stable to air, and exhibit a clean thermal decomposition to gold metal. Both dimethylgold trifluoroacetylacetonate, $Me_2Au(tfac)$ and dimethylgold hexafluoroacetylacetonate, $Me_2Au(hfac)$, offer higher ambient vapor pressures than the nonfluorinated analogue. All three organogold complexes decompose at sufficiently low temperature to permit the LCVD of gold onto some polymeric substrates. A comparison of the deposition rates, resistivities, and the quality of the metal produced is made for the LCVD of gold from these three related precursors.

Experimental

The gold complexes utilized throughout this study were synthesized according to the literature procedure of Brain and Gibson (4). Dimethylgold iodide dimer was prepared from tetrachloroauric acid and then reacted with the potassium salt of acetylacetone, trifluoroacetylacetone, or hexafluoroacetylacetone.[1] The final products were purified by careful distillation or sublimation, as appropriate. The physical properties for the three gold complexes are given in Table I. Differential scanning calorimetry (DSC) was performed on the neat complexes to determine the temperatures of decomposition. Vapor pressures were determined with a capacitance manometer after several freeze-pump-thaw cycles.

In the laser deposition experiments, the 514.5 nm line from an argon ion laser was utilized (Coherent Innova 20). The beam was attenuated with a half-wave plate combined with a polarizing prism and was focused with a single, plano-convex lens (10 cm focal length). The laser power was monitored with a Newport photodiode (Model 815) through the use of a beamsplitter while the experiment was in progress. The power readings were corrected for absorbance/reflectance losses at the optical interfaces. At the substrate, the power density was calculated after accounting for the focal spot diameter (45 μm for the 10 cm lens).

The substrate was contained in a vacuum cell (stainless steel) fitted with an optical quartz window and vacuum valve. Neat gold complex was placed into the cell prior to evacuation and the cell was pumped to a background pressure of 10^{-4} torr with a turbomolecular pump; cooling of the cell during pump down was required to prevent evaporation of the highly volatile $Me_2Au(hfac)$ complex. The cell was mounted on a motorized stepper stage (Ealing) and could be scanned through the focused beam to "write" lines of metal. The beam was kept normal to the substrate at all times and focused onto the substrate surface. All of the depositions were carried out with the cell at room temperature (24°C).

The heights and widths of deposited gold spots, used for rate measurements, were determined from optical and scanning electron microscopy (SEM), respectively. The electrical resistances were measured on a Magnetron Instrument (Model M-700) four-point probe equipped with a Probex head. Typically, a gold line was laser deposited across evaporated gold pads (3000Å). Cross-sectional areas were calculated from profilometer traces and used to calculate line resistivities. Annealing of laser deposited lines was achieved by placing the sample in a quartz tube in a convection furnace.

Table I. Properties of gold complexes. Melting point and ambient vapor pressure of the gold complexes

Complex	T_m (°C)	P_{25} (mT)
1a	82	9
1b	40	40
1c	~5	350

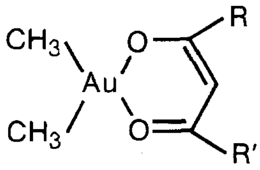

Complex	Structure	Abbreviation
1a	R = R' = CH_3	$Me_2Au(acac)$
1b	R = CH_3 R' = CF_3	$Me_2Au(tfac)$
1c	R = R' = CF_3	$Me_2Au(hfac)$

Fig. 1. Molecular structure of the gold complexes utilized in this study. The incorporation of fluorine atoms in the acetylacetonate ligand is depicted by structures 1b and 1c.

Scanning Auger electron spectroscopy (SAES) of the deposited gold was performed at Surface Science Laboratories, Mountain View, California. Argon ion sputtering was employed to depth profile the gold deposits.

Results and Discussion

Complex properties.—The synthesis of $Me_2Au(acac)$, 1a, was reported as early as 1939 (4). The incorporation of fluorine atoms into the acetylacetonate ligand affords the synthesis of $Me_2Au(tfac)$, 1b, and $Me_2Au(hfac)$, 1c, complexes as reported by Kochi in 1978 (6). Fluorinated organics are known to have higher ambient vapor pressures when compared to their hydrocarbon analogues, presumably by decreased van der Waals and hydrogen bonding interactions (7). As expected, the fluorinated gold complexes have increased vapor pressures (Table I) under ambient conditions. Differential scanning calorimetry (DSC) of the neat complexes shows that all three gold complexes undergo exothermic decomposition beginning at 160°C. Although the decomposition temperatures are similar, the activation energy to decomposition may be quite different. The increasing volatility of the complexes with increasing temperature makes an accurate measure of the decomposition enthalpy (ΔH_d) difficult.

The purified, neat materials are quite stable in air at 0°C for long periods of time. However, at elevated temperatures or in protic solvents, decomposition is observed with reductive elimination (8) of ethane and sub-

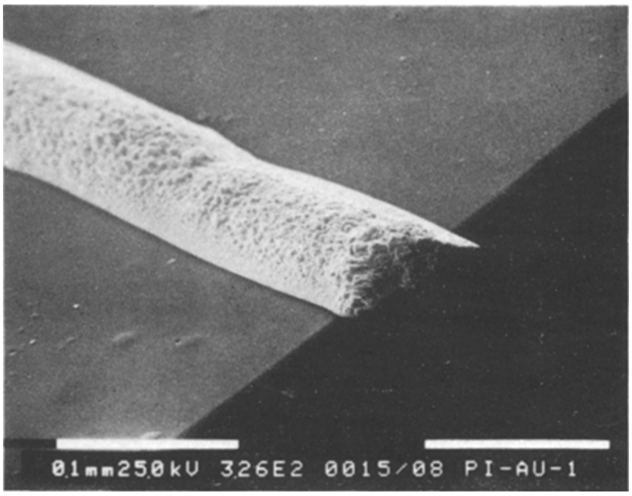

Fig. 2. Gold line deposited on du Pont RC5878 from 1a at 2 μm/s. Line is 90 μm wide and 20 μm in height.

---

[1] A modification of the procedure in Ref. (5) was used.

sequent precipitation of gold (9). The relatively low decomposition temperature of the neat complexes enables the facile deposition of gold onto polymeric substrates which possess a high glass transition (10) temperature (T_g) without damage to the polymer. The deposition of gold onto a commercially available polyimide (du Pont RC5878) is shown in Fig. 2. The high vapor pressures at ambient temperatures and low thermal decomposition temperatures makes these three complexes highly desirable precursors for the LCVD of gold.

Rates of Deposition

Rates of gold deposition were determined for the three compounds by growing spots of gold onto silicon wafers with a thermally grown SiO_2 layer (2800Å). Deposition rates were compared utilizing the ambient vapor pressures of the precursors while all other experimental conditions were identical.

Previous studies on the growth of gold deposits with time were shown to increase with increasing laser power for 1a (3). The growth of gold spots occurs in two distinct stages; the induction or nucleation stage and the steady growth stage. The nucleation time is often long, but is observed to decrease with increasing laser power. Thus, a higher laser power induces a higher local surface temperature, a shorter nucleation time, and a wider deposited spot. As seen in Fig. 3, the time for the initiation of deposition decreases in going from 1a to 1c, for an identical substrate, laser power, and focal spot size. The decreased induction time suggests that the formation of a thin, nucleation layer is dependent on the vapor phase concentration. After the initiation of deposition, the vapor phase concentration will be a rate-determining factor as demonstrated in these studies for the LCVD of gold.

Deposition at elevated cell temperatures was found to yield faster rates of deposition (3) with 1a. The enhanced rate of deposition was attributed to the increased vapor pressure of the complex, consistent with the models of Ehrlich (11) and Kodas (12). A similar increase in vapor pressure is achieved in these experiments without changing the cell temperature; the three organogold complexes have different ambient vapor pressures, but similar decomposition temperatures. Thus, under identical experimental conditions, deposition of gold from 1b and 1c showed increased rates of deposition when compared to 1a (Fig. 3), as expected based upon their relative vapor pressures (Table I).

Using the kinetic model of Ehrlich and Tsao (11, 13) we can calculate theoretical rates of gold deposition, assuming a hard-sphere approximation (14), to compare with our experimentally determined rates. In the simplified rate expression, where the mean free path (l) is much greater than the focal spot diameter, the rate, r, is given by

$$r = \frac{D\{R\}}{l} = \frac{\{R\}\,\epsilon\nu}{2}$$

where $\{R\}$ is the concentration of precursor at its room temperature vapor pressure, ϵ is the probability for reaction of a precursor molecule upon collision with the locally heated substrate, and ν is the rms velocity of the precursor at room temperature. Values of rates (r), in which ϵ is unity, are given in Table II, as well as values for $\{R\}$ and ν. If ϵ is similar for the three gold complexes, then the rates are governed predominantly by the vapor phase concentration, for identical laser conditions. Assuming that ϵ is equal for the three compounds, the calculated rates of deposition for 1b and 1c are 4.3 and 33 times faster, respectively, than the rate for 1a. This calculated rate trend is similar to that observed experimentally as shown in Fig. 3; the vertical growth rates are 0.45 μm/s (4.5 times) for 1b, and 2.5 μm/s (25 times) for 1c as compared to 0.1 μm/s for deposition from 1a. These vertical growth rates indicate that the deposition of gold is governed predominantly by the gas phase concentration and that ϵ is similar for the three organogold complexes.

Table II. Calculated physical properties. Calculated values of $\{R\}$ and ν for the gold complexes. The calculated values of r assume $\epsilon = 1.0$

Complex	$\{R\}$ mol/cm³	ν cm/s	r atom/cm²-s
1a	2.8×10^{14}	1.4×10^4	2.0×10^{18}
1b	1.3×10^{15}	1.3×10^4	8.5×10^{18}
1c	1.1×10^{16}	1.2×10^4	6.6×10^{19}

Surface Analyses and Resistivity Measurements

Resistivities of gold lines were examined at several laser powers, scan speeds, and after a post-annealing step. The laser power has a minimal effect on line resistivity, but does increase the width of the line and the observed grain size of the metal. Also, the laser power can alter the deposit shape, such that volcano (15) profiles are noted at high laser powers. This is especially true for 1c in comparison to both 1a and 1b on SiO_2 over silicon and may result from a lower desorption temperature for 1c. Scan speeds of <10 μm/s result in thick lines with the thickness being determined by the rate of deposition and thus, the precursor complex (*i.e.*, 1c > 1b > 1a). At a constant laser power, increasing the scan speed results in an increased resistivity for deposition from 1a (3). The decreasing line thickness (<0.5 μm) with the increasing scan speed results in gold lines which become increasingly discontinuous and finally, are no longer conducting (>40 μm/s). Resistivities of gold lines deposited from 1b and 1c, however, were inversely affected by the scan speed. Fast scan speeds (≥5 μm/s) produced lines of

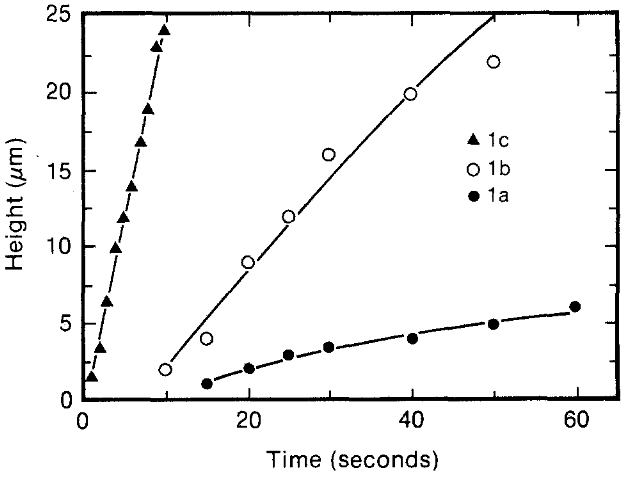

Fig. 3. Thickness of deposited gold as a function of irradiation time; comparison of the three complexes under identical laser conditions (1.0×10^5 W/cm²) onto SiO_2 over silicon at room temperature (24°C).

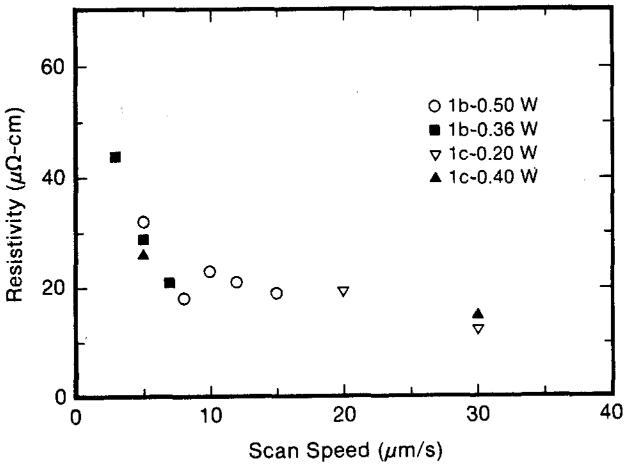

Fig. 4. Calculated resistivities as a function of scan speed for gold lines deposited from 1b and 1c before annealing.

sufficient thickness (>2 μm) which had lower resistivities when compared to lines written at slow scan speeds (Fig. 4) for one laser power. The slower scan speeds result in thicker lines and may possess a poor morphology for electrical conduction. The number density of voids (16) in evaporated films is related to the rate of metal deposition and an analogous situation may exist for the LCVD of metals.

The purity of the deposited gold from 1a was found to be 96-98% based upon scanning Auger and x-ray photoelectron emission data (3). Both 1b and 1c produce gold deposits which contain trace amounts of carbon and oxygen, but have been observed to be ≥ 95% purity after depth profiling (100Å)[2] with argon. The calculated resistivities of gold lines deposited from 1b are shown in Fig. 4 (0.50W) and these lines had gold concentrations of 95-100% with no correlation to scan speed. Thus far, the deposit purity does not vary with laser power and/or scan speed within experimental error. This would seem to indicate that the morphology of the gold film, rather than purity, will determine the observed resistivities.

Resistivities can be reduced with a post-annealing step (3) through a reduction in the number of defects within the film (16). Typically, temperatures of 300°-350°C for 30 min in air were used to anneal the films. Interestingly, annealing reduces the resistivities of lines deposited from 1a, 1b, and 1c, but the observed decrease is smaller for lines deposited from 1c when compared to lines deposited from 1a and 1b. Similar behavior upon annealing has been observed for gold films grown by conventional CVD (17) from both 1b and 1c. Once again, this behavior can be attributed to the film's morphology. The grain size of gold particles deposited by CVD from 1b are small, while larger grained deposits are observed from 1c. Lines deposited by LCVD from all three gold precursors generally have resistivities which are two to 20 times bulk gold (2.44 μΩ-cm) and can be reduced to two to five times bulk material after annealing.

Recent temperature measurements and calculations (18) have shown that the surface temperature does not vary greatly with scan speed on SiO_2 over silicon. However, the surface temperature is strongly influenced by the thickness of the gold line being deposited; thus, the surface temperature will decrease with increasing thickness of the deposited line as a result of thermal conduction (19). At the slow scan speeds, deposition of a thicker line occurs simultaneously with a decrease in surface temperature. The lowered surface temperature could result in a minimum of thermal annealing, a change in deposit morphology, and ultimately, in higher observed resistivities for lines deposited from 1b and 1c. For lines deposited from 1a, the surface temperature remains high with the increasing scan speed, but the lines become discontinuous due to a decreasing line thickness.

Conclusions

LCVD of gold metal from 1a, 1b, and 1c has been demonstrated. The deposition rates are strongly dependent upon the vapor pressure and therefore, the precursor utilized. Relative experimental and theoretical rates of deposition have shown good agreement. The low deposition temperatures allow the deposition of gold to be achieved, by a pyrolytic process, onto thermally sensitive substrates. The purity of metal is high and highly conducting gold lines can be produced on several substrates; a post-annealing step may be utilized to reduce the line resistivities. The deposition process can be tailored by the choice of gold complex, laser power, and scan rates for a specific application.

Acknowledgments

Special thanks are given to R. Seimens for the differential scanning calorimetry measurements and to R. Jackson and P. Comita for many helpful discussions.

Manuscript submitted Nov. 17, 1986; revised manuscript received April 17, 1987.

IBM Almaden Research Center assisted in meeting the publication costs of this article.

REFERENCES

1. R. J. Von Gutfeld, E. E. Tynan, R. L. Melcher, and S. E. Blum, *Appl. Phys. Lett.*, **35,** 651 (1979); R. J. Von Gutfeld, R. E. Acosta, and L. T. Romankiw, *IBM J. Res. Dev.*, **26,** 136 (1982).
2. M. E. Gross, A. Applebaum, and K. J. Schnoes, *J. Appl. Phys.*, **60,** 529 (1986); M. E. Gross, G. J. Fisanick, P. K. Gallagher, K. J. Schnoes, and M. D. Fennell, *Appl. Phys. Lett.*, **47,** 923 (1985); G. J. Fisanick, M. E. Gross, J. B. Hopkins, M. E. Fennell, and K. J. Schnoes, *J. Appl. Phys.*, **57,** 1139 (1985).
3. T. H. Baum and C. R. Jones, *Appl. Phys. Lett.*, **47,** 538 (1985); T. H. Baum and C. R. Jones, *J. Vac. Sci. Technol.*, **B4,** 1187 (1986).
4. F. H. Brain and C. S. Gibson, *J. Chem. Soc.*, 762 (1939).
5. R. G. Charles, *Org. Syn.*, *IV*, 869 (1965).
6. S. Komiya and J. K. Kochi, *J. Am. Chem. Soc.*, **99,** 3695 (1978).
7. W. A. Sheppard and C. M. Sharts, "Organic Fluorine Chemistry," pp. 40-43, W. A. Benjamin, Inc., New York (1969); T. M. Reed, "Fluorine Chemistry," Vol 5, pp. 133-236, Academic, New York (1964); W. R. Wolf, R. E. Sievers, and G. H. Brown, *Inorg. Chem.*, **11,** 1995 (1972).
8. G. K. Anderson, *Adv. Organomet. Chem.*, **20,** 89 (1982).
9. R. B. Klassen and T. H. Baum, Unpublished results (1986).
10. F. W. Billmeyer, "Textbook of Polymer Science," Wiley, New York, pp. 207-211 (1971).
11. D. J. Ehrlich and J. Y. Tsao, *J. Vac. Sci. Technol. B*, **1,** 969 (1983).
12. T. T. Kodas, T. H. Baum, and P. B. Comita, *J. Appl. Phys.*, **62,** 281 (1987).
13. C. R. Moylan, T. H. Baum, and C. R. Jones, *Appl. Phys. A*, **40,** 1 (1986).
14. R. S. Berry, S. A. Rice, and J. Ross, "Physical Chemistry," p. 1073, John Wiley & Sons, Inc., New York (1980).
15. S. D. Allen, *J. Appl. Phys.*, **52,** 6501 (1981); S. D. Allen, R. Y. Jan, R. H. Edwards, S. M. Mazuk, and S. D. Vernon, *SPIE Proc.*, **459,** 42 (1984).
16. L. I. Maissel, "Handbook of Thin Film Technology," Chap. 13, pp. 13-28, McGraw-Hill, Inc., New York (1970).
17. C. E. Larson, T. H. Baum, and R. L. Jackson, *This Journal*, **134,** 266 (1987).
18. T. T. Kodas, T. H. Baum, and P. B. Comita, *J. Appl. Phys.*, **61,** 2749 (1987).
19. K. Piglmayer, J. Doppelbauer, and D. Baurle, *Mat. Res. Soc. Symp. Proc.*, **29,** 47 (1984).

---

[2] This is an estimated depth for argon ion sputter based upon a standard film of Ta_2O_5. Gold may sputter two to three times as rapidly as the standard.